Impact of ion irradiation, elemental doping and coating cycles on structural characteristic parameters of nanocrystalline VO_2 thin films

G.R. Khan ✉

Nanotechnology Research Laboratory, Department of Physics, National Institute of Technology Srinagar, Hazratbal 190006, Kashmir, India
✉ *E-mail: grkhan786@gmail.com*

Published in Micro & Nano Letters; Received on 22nd March 2019; Revised on 10th July 2019; Accepted on 2nd August 2019

The origin of the structural phase transition in vanadium dioxide (VO_2) has been the subject of immense disagreement in spite of decades of research carried out to comprehend this intriguing phenomenon. Diverse models have been developed to elucidate the obscure theory in order to corroborate assorted experimental results. Herein, the influence of swift heavy ion irradiation, elemental doping and coating cycles on the structural properties of thin films synthesised by sol–gel technique and deposited by spin coater on alumina and glass substrates is investigated. The thin films were characterised by X-ray diffractometry and the XRD spectra obtained at 1E11, 5E11, 1E12 ion beam fluances of 200 MeV Ag^{9+}-ion irradiation; at 1, 3, 5% of Mo^{6+}-ion doping and at different spin coating cycles were analysed to probe the influence of these effects on the structural characteristic parameters of nanocrystallites in VO_2 thin films. This aspect of VO_2 thin films has not been investigated to its full capacity and consequently, not reported in the scientific literature.

1. Introduction: Vanadium (V), a group-5 transition element, has atomic number 23 and electron configuration [Ar] $3d^3 4s^2$ with 3d and 4s sub-shells partially filled. Vanadium dioxide (VO_2), a strong electron correlated metal oxide, has been the focus of extensive research because it undergoes first-order thermal reversible structural phase transition between high stable, less symmetric (P21/c), low temperature monoclinic (M1) semiconducting phase and low stable, high symmetric (P42/mnm), high-temperature tetragonal rutile (R) metallic phase (SMT) [1]. This SMT of VO_2 is scientifically exciting and technologically appealing around a phase transition temperature (T_t) of 341 K closest to room temperature than any other material discovered to date in its un-irradiated, un-doped, and bulk state [2–5].

Obviously, VO_2 has emerged as a desirable contender for a variety of modern-day technological applications such as variable reflectance mirrors, microbolometers, thermo-optical switches, thermo-optical light modulators, energy storage media, energy-conserving coatings, and temperature sensors [2].

In R phase, V–V atoms are equally spaced along linear chains in the c_R direction and stabilise to a body-centred tetragonal lattice with a pair of V atoms per unit cell with each V atom engulfed by a regular octahedron formed by 6 O atoms. M1 phase exists in a double size monoclinic unit cell evolved by collapsing of the tetragonal structure and pairing and tilting of V atoms with respect to the *c*-axis of R phase through distorted O octahedron exhibiting alternating V–V spaces with equivalent direction of $a_{M1} = 2c_R$ [6, 7], as displayed in Fig. 1.

The fundamental phenomenon behind SMT in VO_2 stands controversial because it has characteristics that cannot be completely explained either by structural Peierls model or by electron-correlated Mott–Hubbard model. If SMT in VO_2 emerges due to structural transition, then SMT has a band-like nature theorised by Peierls transition [8–15], but if structural transition is only an associated effect of the charge carrier supported SMT, then it is a Mott transition [16–20] or Mott–Hubbard transition [21–25]. Although several features reveal that SMT pops up due to the critical carrier concentration in which electron correlations contribute predominantly whereas other features imply that SMT arises due to the interaction of structural disorders and Coulomb correlations. This explanation moves away from both Mott and Peierls transitions in competition and, therefore, may be dubbed to some extent as Mott–Peierls transition [26–30]. Apart from R and M1 structural phases, the existence of triclinic (T) and monoclinic (M_2) structural phases further exacerbate the dilemma [14, 31–41].

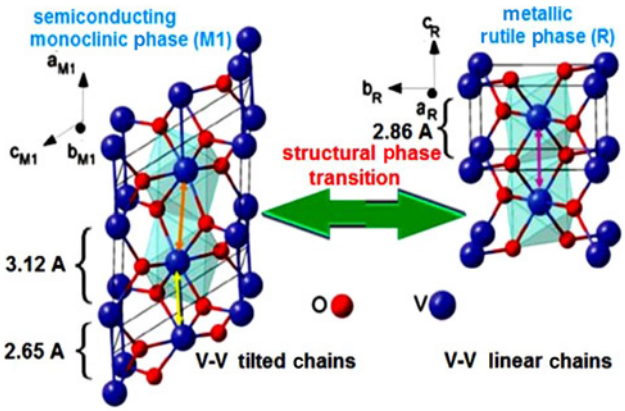

Fig. 1 *Transformation between rutile and monoclinic crystalline phases of VO_2*

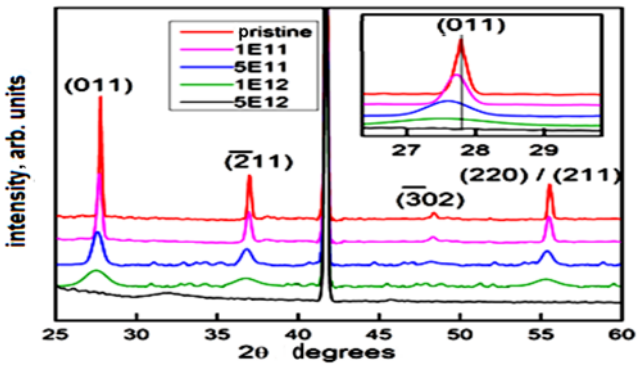

Fig. 2 *XRD spectra of un-irradiated and 200 MeV Ag^{9+}-ion irradiated VO_2 thin films at different fluences. Inset shows broadening and shifting of (011) peak towards lower diffraction value*

doi: 10.1049/mnl.2019.0186

Table 1 SCP of VO_2 thin films irradiated by 200 MeV Ag^{9+}-ions with increasing ion beam fluence casted on alumina substrates by eight spin coating cycles at 3000 rpm for 30 s and corresponding to (011) intensity peak of XRD spectra

Fluence, ions/cm^2	2θ, deg.	I_{011}, Arb. units	d_{011}, Å	$\beta \times 10^{-4}$, rad	D, nm	$\varepsilon \times 10^{-4}$	S, m^{2}g^{-1}	L	L_P
0	27.791	716.6	3.2076	32.15	43.93	32.49	29.88	4.46	31.84
1E11	27.727	383.3	3.2148	61.37	23.01	62.16	57.05	4.48	32.00
5E11	27.611	191.1	3.2281	124.70	11.32	126.87	115.96	4.52	32.28
1E12	27.591	80.5	3.2303	256.07	5.51	260.73	238.23	4.53	32.33

In this Letter, nanocrystalline VO_2 thin films grown by sol–gel process and spin-coated on alumina/glass substrates were characterised by X-ray diffractometry for studying the structural characteristic parameters (SCP) of the thin films. The XRD spectra obtained from SHI irradiated, Mo-doped and pristine nanosized crystallites of VO_2 thin films were analysed. Such studies bear importance in the wake of observing the changes in structural features ranging from one effect to the other. Due to the scarcity of relevant XRD data, these characteristics of VO_2 thin films have not been meticulously probed. The variations of SCPs under diverse conditions are essential and XRD analysis should offer a viaduct between experimental results and theoretical understanding of the transition. The aim of this endeavour is to present the influence of irradiation with 200 MeV Ag^{9+}-ions at diverse beam fluances, doping with Mo^{6+}-ions at various percentages and casting of substrates at different spin coating cycles on SCP of nanocrystallites of VO_2 thin films.

2. Film fabrication: Pristine VO_2 films were prepared via sol–gel method by dissolving 0.3 g of the V_2O_5 in 30 ml of 30% H_2O_2 solution (Sigma Aldrich) through heating and stirring at 60°C till thermal decomposition of H_2O_2 took place. Following ageing of 24 h, the V_2O_5 gel was spin-coated on cleaned glass substrates. One and ten successive coatings were performed at a spin speed of 6000 rpm for 30 s on separate glass substrates [2]. Doped VO_2 films with 0, 1, 3 and 5% of Mo^{6+}-ions were synthesised by the same process with the addition of an appropriate amount of MoO_3 (Sigma Aldrich) and melted in a ceramic crucible at 800–900°C for 25–30 min in a muffle furnace in an ambient atmosphere. The molten liquid was immediately transferred into distilled water at 80°C with constant stirring for 3–5 h and then the solution was homogenised in an ultrasonic bath for >1 h. Subsequent to the ageing of 24 h, the V_2O_5 gel was spin-coated on each cleaned alumina substrate at a spin rate of 3000 rpm for 30 s by three successive coatings [3]. Thin films of VO_2 for irradiation were similarly fabricated by melting 3.7 g of V_2O_5 (Sigma Aldrich, purity 99.9%) and 5.40 g of $H_2C_2O_4{\cdot}2H_2O$ (Sigma Aldrich) in a ceramic crucible at 750°C in a muffle furnace for 30 min and then poured quickly into a beaker containing 30 ml of deionised water placed on a magnetic stirrer. 10 ml of freshly prepared polyvinyl alcohol (0.2 g) solution was added drop-wise to the above solution and stirred for the next 30 min continuously at room temperature. After aging for one day, the resultant sol was cast on cleaned alumina substrates at a rate of 3000 rpm for 30 s using a spin coater (Spin-NXG-P1:Apex Instruments). Eight successive coatings of V_2O_5 gel were performed on every alumina substrate [4].

After each casting cycle, all V_2O_5 gel films were dried at 80°C for 15–20 min on a hot plate to eliminate excessive water and organics. All pristine and Mo^{6+}-doped thin films were crystallised and reduced to VO_2 by annealing at 450°C for 4 h in a mixed environment of argon (95%) and hydrogen (5%) in a programmable tubular furnace (Nabertherm GmbH Tube furnace:RHTC80) with a heating and cooling rate of 3°C/min.

3. Film irradiation: The structural characteristics of VO_2 thin films also depend on their defects [42] and to tune the structural characteristics, defects can be induced by swift heavy ion (SHI) (MeV) irradiation [43]. Since the distribution of created defects is not uniform, the role played by defects in structural modification of VO_2 becomes important. The distinctive feature of SHI is the generation of ion tracks of nanosized cylindrical zones in addition to a cluster of point defects and annealing defects depending upon the target material besides mass and energy of the irradiated ions. The number density of ion tracks, microstructures and defects can be controlled by irradiated ion beam parameters such as fluence (ions/cm^2), ion-type and ion-energy [44].

VO_2 thin films deposited on alumina substrates were irradiated by 200 MeV Ag^{9+}-ions from 15 UD Pelletron Accelerator (IUAC, New Delhi) at ion beam fluences of 1E11, 5E11, 1E12, and 5E12 ions/cm^2 [4]. The choice of Ag^{9+}-ion is not arbitrary but based on its higher mass and the energy simulated by the SRIM-2013 code [45]. The irradiation was carried out at a high vacuum at a base pressure of 2×10^{-6} Torr, a beam current of ~0.1 particle nano ampere (*PnA*), a beam-spot size of 1 mm diameter, and the film was scanned over the entire film area using a magnetic scanner.

4. XRD measurements: The XRD can be employed in the SCP Letter of nanocrystalline thin films as there exists an explicit atomic arrangement in a crystal. The Bragg peaks attain a finite width owing to the instrumental resolution, nanograin size and indiscriminate strains. The full-width at half-maximum (FWHM) of the XRD peaks is a measure of the broadening of Bragg peaks that divulge information about nanocrystallite size, mosaic broadening and microstrain. The positions, shapes, and intensities of the measured peaks reveal the crystal structure of VO_2 films and were investigated by using a Bruker D8 Advance X-ray diffractometer with Cu-Kα radiation of 0.15406 nm for the rotating angle of 2θ in the range of 20–70° at an X-ray source scan speed of 0.5°/min.

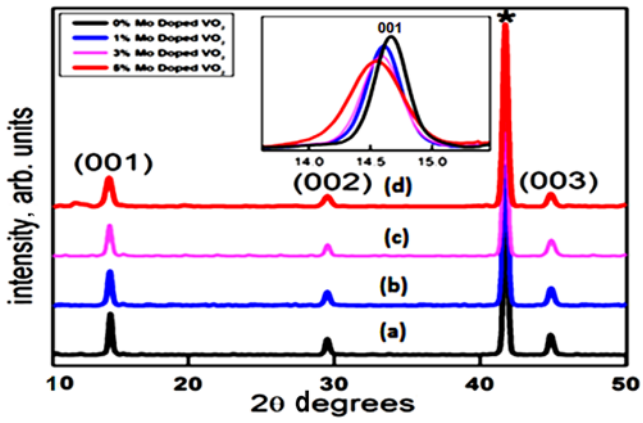

Fig. 3 *XRD spectra of*
a 0%
b 1%
c 3%
d 5% Mo^{6+}-doped VO_2 thin films. Inset shows broadening and shifting of (001) peak towards lower 2θ with Mo^{6+}-doping

Table 2 SCP of Mo^{+6} -doped VO_2 thin films with increasing percentage casted on alumina substrates by three spin coating cycles at 3000 rpm for 30 s corresponding to (001) intensity peak of XRD spectra

Mo-doping, %	2θ, deg.	I_{001}, Arb. units	d_{001}, Å	$\beta \times 10^{-4}$, rad	D, nm	$\varepsilon \times 10^{-4}$	S, m^2g^{-1}	L	L_P
0	14.648	304.4	6.0425	54.80	25.23	106.60	52.03	15.51	120.11
1	14.610	278.5	6.0581	57.07	24.22	111.30	54.20	15.59	120.75
3	14.580	250.5	6.0705	65.62	21.06	128.25	62.33	15.65	121.26
5	14.550	233.7	6.0830	86.39	16.00	169.13	82.04	15.71	121.68

5. Irradiation effect: A characteristic diffraction pattern is produced by plotting the X-ray intensities against 2θ scanned values of the crystalline films. XRD plots of un-irradiated and 200 MeV Ag^{9+}-ion irradiated VO_2 thin films at different fluences in the 2θ range of 25–60° are displayed in Fig. 2. Diffraction pattern of these VO_2 thin films samples can be assigned to Monoclinic (M) phase [JCPDS Card No. 82-0661, space group P21/C] with lattice constants as $a = 5.743$ Å, $b = 4.517$ Å, $c = 5.375$ Å, $\gamma = 90°$ and $\beta = 122.6°$. At $2\theta = 41.71°$, the sharp Bragg peak occurs due to reflections from the (0006) plane of the Al_2O_3 substrate. Bragg peaks at $2\theta = 27.88°$, 37.70°, 48.42° and 55.51° emerge as a result of reflections from (011), (210), (302) and (211/220) planes of the M-phase of VO_2, respectively. The high-intensity peak at 27.88° reveals that the films are well (011) oriented and belongs to the lowest energy of the M phase. An exaggerated image of (011) peak is portrayed as an inset of Fig. 2 which elucidates that the peak intensity diminishes, peak width expands and peak position shifts towards the lower value of diffraction angle with the augmentation of the beam fluence.

The average nanocrystallite size (D) is estimated by Debye–Scherrer equation, $D = 0.89\lambda/\beta\cos\theta$, ($\lambda = 0.15406$ nm), the microstrain (ε) computed from the Stokes–Wilson relation, $\varepsilon = \beta/(4\tan\theta)$, the specific surface ($S$) area determined from the Brunauer–Emmet–Teller (BET) equation, $S = 6/(\rho D)$, where ρ is the material density (4.571 g/cm^3), the Lorentz factor (L) calculated from the equation $L = 1/(4\sin^2\theta\cos\theta)$ and the Lorentz polarisation factor (L_p) worked out by the formula $L_p = (1 + \cos^2 2\theta)/(\sin^2\theta\cos\theta)$. Table 1 shows the variation of position (2θ), interplanar space (d), intensity (I), FWHM (β), nanocrystallite size (D), microstrain (ε), specific surface area (S), Lorentz factor (L) and Lorentz polarisation factor (L_p) corresponding to (011) peak of the samples. A variation of these parameters can be explained as follows. SHI irradiation causes disordered regions in the films, which increase with increasing fluence. No sharp peak subsists at fluence 5E12 ions/cm^2 thereby demonstrating the amorphous nature of this film with no grain boundary. The extinction of the peak at this fluence is attributed to the overlapping of disordered regions. The observed minor shift of (011) peak in the direction of smaller 2θ values occurs due to the relaxation of the compressive strain upon the creation of disordered regions through the variation of d_{hkl} in irradiated films in contrast to the un-irradiated film. The broadening of peaks is affected by any change of the crystal structure by microstrains present in thin films. The reduction in D is attributed to the irradiation-induced grain splitting effect. Hence, the creation of disordered regions by SHI irradiation clearly shows the change in the relative XRD peak intensities which in turn play a pivotal role in the SCP of VO_2 films.

6. Doping effect: Another well-established technique to modulate the SCP is to induce an appropriate dopant that either influences or impedes phase transformations by careful stabilisation. In VO_2, a commonly employed technique for tuning SCP for practical applications has been the doping with those transition metal ions that can exert influence in its crystallographic structure. It is envisaged that the band structure must be sensitive to changes in the lattice produced by the incorporation of impurity ions into VO_2 crystals. VO_2 microstructures have been achieved by doping them with high valance metal ions that generate a donor like a defect. Molybdenum (Mo) is one of the metal ions that have relatively broad tunability with less dopant concentration in VO_2 thin films and is, therefore, considered the most suitable dopant.

X-ray diffraction patterns of the final samples were recorded at a scan speed of 0.5°/min at room temperature in the 2θ range of 10°–50°. The XRD spectra of 0, 1, 3 and 5% Mo^{6+}-doped VO_2 thin films are shown in Figs. 3*a–d*, respectively. The diffraction pattern of the samples can be indexed to a monoclinic VO_2 phase. With a different percentage of Mo^{6+} ions in the films, no considerable discrepancies were observed in the crystal structure. This is consistent with the results achieved through pulsed laser deposition [46] and RF-sputtering [47] techniques for Mo-doped VO_2 thin films deposited on single-crystal alumina substrates. The sharp peak (*) at 41.71° matches well with diffraction from (0006) plane of alumina substrate. The intensity peaks at 14.63°, 29.50° and 44.90° commensurate with reflections from (001), (002) and (003) planes of the M phase which signify that highly textured VO_2 films have developed along the c-axis. Analogous growth orientation was observed by Jian *et al.* [48]. Inset of Fig. 3 shows broadening as well as the slight shift of (001) intensity peak towards lower 2θ value with Mo-doping indicating an enhancement of adjacent d-spacing according to Bragg law. Table 2 presents the values of SCP corresponding to the (001) peak of the samples. It is evident from the table that d and β increase, whereas D decreases with the increase of doping percentage.

7. Size effect: A consequential stimulation by the confinement of electrons in low-dimensional nanostructures offers a distinctive opportunity to tune the properties and functionalities of nanostructures for a wide range of potential applications. Thus, the immense significance is attached to the studies of size effect on the SCP of thin films. Here, we study the impact of size effect in VO_2 thin films by a comparative study of crystal structural analysis of pristine VO_2 thin films deposited on glass substrates by 1 and

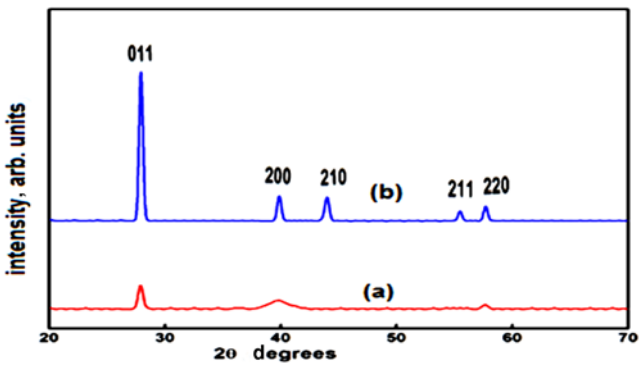

Fig. 4 *XRD spectra of pristine VO_2 thin films for*
a 1
b 10 spin coating cycles

doi: 10.1049/mnl.2019.0186

Table 3 SCP of pristine VO_2 thin films deposited on glass substrates by 1 and 10 spin coating cycles at 6000 rpm for 30 s corresponding to (011) intensity peak of XRD spectra

Coating cycles	2θ, deg	I_{011}, Arb. units	d_{011}, Å	$\beta \times 10^{-4}$, rad	D, nm	$\varepsilon \times 10^{-4}$	S, m^2g^{-1}	L	L_P
1	27.90	60.20	3.1953	91.11	15.51	91.69	84.63	4.43	31.58
10	27.94	848.9	3.1908	71.56	19.75	71.91	66.46	4. 42	31.48

10 spin-coating cycles of VO_2 by X-ray diffractometry. Fig. 4 displays the XRD patterns of these thin films at room temperature in the 2θ range of 20°–70°. The diffraction peaks of the films can be indexed to an M symmetry of VO_2. As is apparent from XRD patterns of both the films, a high-intensity peak appearing at 27.72°corresponds to (011) plane, and two low-intensity peaks at 39.5° and 57.63° correspond to (200) and (220) planes, respectively. Besides these three peaks, the XRD patters of the thin-film cast at 10 spin-coated cycles exhibit two additional peaks at 44° and 55.5° that can be allocated to reflections from (210) and (211) planes, respectively. The high-intensity peak observed at (011) plane with regard to other peaks reveals that VO_2 prefers to align along (011) plane on glass substrate being the low-energy plane of the monoclinic phase of VO_2. Table 2 shows the variation of different SCP is corresponding to the main (011) peak. From the table, it is apparent that both d as well as β increase with the decrease of the crystallite size of the thin film.

8. Overall impact: The most significant component of XRD profiling is that the intensity of the diffraction peaks is distinct from different angles as well as for different planes. This is attributed to the presence of the Lorentz-polarisation factor which controls the intensity of diverse peaks corresponding to the dissimilar angles and unlike planes. Interplanar spacing has a certain spread rather than a particular value that causes broadening of the peak. The peak broadening in thin films is due to a decrease in the crystalline size and development of microstrains. Microstrain is broadening crops up from non-uniform lattice distortions due to lattice defects in crystalline materials that increase with the decrease of nanocrystalline size. Microstrain also arises due to the lattice mismatch between the film and the substrate. Variation in crystalline size as well as in microstrain is responsible for inducing changes in the lattice parameters, which lead to modification of the SCP of thin films. Tables 1–3 displaying variations of SCP of irradiated, doped and pristine VO_2 thin films, in general, reveal that D decreases whereas d, β, ε, S increase with the increase in ion beam fluence, doping percentage and with the decrease of number of spin coating cycles.

9. Conclusions: Summarising, in this Letter, we have investigated the impact of irradiation effect, doping effect, and size effect on the structural characteristic parameters of nanocrystalline VO_2 thin films based on X-ray diffractometery analysis. The films processed through inorganic sol–gel technique were deposited on alumina and glass substrates by spin coating technique. The analysis of XRD profiling of the samples was carried out to determine different structural parameters. A variation of these parameters has shown that the Lorentz-polarisation factor tunes the peak intensity and interplanar spacing expands the peak width. XRD patterns of thin films with large d spacing undergo strong reflections at small diffraction angles due to the Lorentz factor. Lorentz factors which depend on the Bragg angle and on the diffraction geometry have also been determined. It has been shown that crystallite size can be controlled with ion beam fluence, doping percentage and spin coating cycles. It offers an exceptional opportunity to modify the properties and functionalities of VO_2 nanofilms, for a wide range of contemporary technological applications.

Furthermore, tailoring of specific surface area, surface roughness, and film-substrate interface reflections can be envisaged from the presented parameters. It reveals that the precise structural characterisation is vitally important for the evaluation of size and strain-induced effects on the phase transition, film-substrate interface and internal structure of the VO_2 nanocrystallites.

10. References

[1] Morin F.J.: 'Oxides which show a metal-to-insulator transition at the Neel temperature', *Phys. Rev. Lett.*, 1959, **3**, p. 34

[2] Khan G.R., Ahmad B.: 'Effect of quantum confinement on thermoelectric properties of vanadium dioxide nanofilms', *Appl. Phys. A*, 2017, **123**, p. 95

[3] Khan G.R., Asokan K., Ahmad B.: 'Room temperature tunability of Mo-doped VO_2 nanofilms across semiconductor to metal phase transition', *Thin Solid Films*, 2017, **625**, p. 155

[4] Khan G.R., Kandasami A., Bhat B.A.: 'Augmentation of thermoelectric performance of VO_2 thin films irradiated by 200 MeV Ag9 +-ions', *Rad. Phys. Chem.*, 2016, **123**, p. 55

[5] Khan G.R., Bhat B.A.: 'Quantum size effect across semiconductor-to-metal phase transition in vanadium dioxide thin films', *IET J. Micro Nano Lett.*, 2015, **10**, p. 607

[6] Andersson G.: 'The crystal structure of vanadium dioxide', *Acta Chem. Scand.*, 1956, **10**, p. 623

[7] Goodenough J.B.: 'The two components of the crystallographic transition in VO_2', *J. Solid State Chem.*, 1971, **3**, p. 490

[8] Goodenough J.B.: 'Direct cation-cation interactions in several oxides', *Phys. Rev.*, 1960, **117**, p. 1442

[9] Adler D., Brooks H.: 'Theory of semiconductor-to-metal transitions', *Phys. Rev.*, 1967, **155**, p. 826

[10] Wentzcovitch R.M., Schulz W.W., Allen P.B.: 'VO_2: Peierls or Mott-Hubbard? A view from band theory', *Phys. Rev. Lett.*, 1994, **72**, p. 3389

[11] Eyert V.: 'The metal-insulator transitions of VO_2: a band theoretical approach', *Ann. Phys.*, 2002, **11**, p. 650

[12] Cavalleri A., Dekorsy T., Chong H.H., *ET AL.*: 'Evidence for a structurally-driven insulator-to-metal transition in VO_2: a view from the ultrafast timescale', *Phys. Rev. B*, 2004, **70**, p. 161102

[13] Haverkort M.W., Hu Z., Tanaka A., *ET AL.*: 'Orbital-assisted metal-insulator transition in VO_2', *Phys. Rev. Lett.*, 2005, **95**, p. 196404

[14] Eyert V.: 'VO_2: a novel view from band theory', *Phys. Rev. Lett.*, 2011, **107**, p. 016401

[15] Xu S., Shen X., Hallman K.A., *ET AL.*: 'Unified band-theoretic description of structural, electronic, and magnetic properties of vanadium dioxide phases', *Phys. Rev. B*, 2017, **95**, p. 125105

[16] Mott N.F.: 'Metal-insulator transition', *Rev. Mod. Phys.*, 1968, **40**, p. 677

[17] Zylbersztejn A., Mott N.F.: 'Metal-insulator transition in vanadium dioxide', *Phys. Rev. B*, 1975, **11**, p. 4383

[18] Imada M., Fujimori A., Tojura Y.: 'Metal-insulator transitions', *Rev. Mod. Phys.*, 1998, **70**, p. 1039

[19] Qazilbash M.M., Brehm M., Chae B.-G., *ET AL.*: 'Mott transition in VO_2 revealed by infrared spectroscopy and nano-imaging', *Science*, 2007, **318**, p. 1750

[20] Nájera O., Civelli M., Dobrosavljević V., *ET AL.*: 'Resolving the VO_2 controversy: Mott mechanism dominates the insulator-to metal transition', *Phys. Rev. B*, 2017, **95**, p. 035113

[21] Pouget J.P., Launois H., D'Haenens J.P., *ET AL.*: 'Electron localization induced by uniaxial stress in pure VO_2', *Phys. Rev. Lett.*, 1975, **35**, p. 873

[22] Imada M., Fujimori A., Tokura Y.: 'Metal-insulator transitions', *Rev. Mod. Phys.*, 1998, **70**, p. 1039

[23] Stefanovich G., Pergament A., Stefanovich D.: 'Electrical switching and Mott transition in VO_2', *J. Phys., Condens. Matter.*, 2000, **12**, p. 8837

[24] Kim H.T., Lee Y.W., Kim B.J., *ET AL.*: 'Monoclinic and correlated metal phase in VO_2 as evidence of the Mott transition: coherent phonon analysis', *Phys. Rev. Lett.*, 2006, **97**, p. 266401
[25] Belozerov A.S., Korotin M.A., Anisimov V.I., *ET AL.*: 'Monoclinic M_1 phase of VO_2: Mott-Hubbard versus band insulator', *Phys. Rev. B*, 2012, **85**, p. 045109
[26] Paquet D., Leroux-Hugon P.: 'Electron correlations and electron-lattice interactions in the metal-insulator, ferroelastic transition in V: a thermodynamical study', *Phys. Rev. B*, 1980, **22**, p. 5284
[27] Biermann S., Poteryaev A., Lichtenstein A.I., *ET AL.*: 'Dynamical singlets and correlation-assisted Peierls transition in VO_2', *Phys. Rev. Lett.*, 2005, **94**, p. 026404
[28] Weber C., O'Regan D.D., Hine N.D., *ET AL.*: 'Vanadium dioxide: a Peierls-Mott insulator stable against disorder', *Phys. Rev. Lett.*, 2012, **108**, p. 256402
[29] Kim S., Kim K., Kang C.J., *ET AL.*: 'Correlation-assisted phonon softening and the orbital-selective Peierls transition in VO_2', *Phys. Rev. B*, 2013, **87**, p. 195106
[30] Nájera O., Civelli M., Dobrosavljević V., *ET AL.*: 'Multiple crossovers and coherent states in a Mott-Peierls insulator', *Phys. Rev. B*, 2018, **97**, p. 045108
[31] Marezio M., McWhan D.B., Remeika J.P., *ET AL.*: 'Structural aspects of the metal-insulator transitions in Cr-doped VO_2', *Phys. Rev. B*, 1972, **5**, p. 2541
[32] Sohn J.I., Joo H.J., Ahn D., *ET AL.*: 'Surface-stress-induced Mott transition and nature of associated spatial phase transition in single crystalline VO_2 nanowires', *Nano Lett.*, 2009, **9**, p. 3392
[33] Zhang S., Chou J.Y., Lauhon L.J.: 'Direct correlation of structural domain formation with the metal insulator transition in a VO_2 nanobeam', *Nano Lett.*, 2009, **9**, p. 4527
[34] Jones A.C., Berweger S., Wei J., *ET AL.*: 'Nano-optical investigations of the metal–insulator phase behavior of individual VO_2 microcrystals', *Nano Lett.*, 2010, **10**, p. 1574
[35] Tselev A., Luk'Yanchuk I.A., Ivanov I.N., *ET AL.*: 'Symmetry relationship and strain-induced transitions between insulating M1 and M2 and metallic R phases of vanadium dioxide', *Nano Lett.*, 2010, **10**, p. 4409
[36] Atkin J.M., Berweger S., Chavez E.K., *ET AL.*: 'Strain and temperature dependence of the insulating phases of VO_2 near the metal-insulator transition', *Phys. Rev. B*, 2012, **85**, p. 020101
[37] Park J.H., Coy J.M., Kasirga T.S., *ET AL.*: 'Measurement of a solid-state triple point at the metal–insulator transition in VO_2', *Nature*, 2013, **500**, p. 431
[38] Ji Y., Zhang Y., Gao M., *ET AL.*: 'Role of microstructures on the M1-M2 phase transition in epitaxial VO_2 thin films', *Sci. Rep.*, 2014, **4**, p. 4854
[39] Hong W.K., Cha S., Sohn J.I., *ET AL.*: 'Metal-insulator phase transition in quasi-one-dimensional VO_2 structures', *J. Nanomater.*, 2015, **2015**, p. 3
[40] Kim H., Slusar T.V., Wulferding D., *ET AL.*: 'Direct observation of the M2 phase with its Mott transition in a VO_2 film', *Appl. Phys. Lett.*, 2016, **109**, p. 233104
[41] Brito W.H., Aguiar M.C.O., Haule K., *ET AL.*: 'Metal-insulator transition in VO_2: a DFT+ DMFT perspective', *Phys. Rev. Lett.*, 2016, **117**, p. 056402
[42] Appavoo K., Lei D.Y., Sonnefraud Y., *ET AL.*: 'Role of defects in the phase transition of VO_2 nanoparticles probed by plasmon resonance spectroscopy', *Nano Lett.*, 2012, **12**, p. 780
[43] Gupta A., Singhal R., Narayan J., *ET AL.*: 'Electronic excitation induced controlled modifications of semiconductor-to-metal transition in epitaxial VO_2 thin films', *J. Mater. Res.*, 2011, **26**, p. 2901
[44] Avasthi D.K.: 'Modification and characterisation of materials by swift heavy ions', *Def. Sci. J.*, 2009, **59**, p. 401
[45] Ziegler J.F.: 'Interactions of ions with matter: SRIM simulation code'. www.srim.org
[46] Wu Z.P., Miyashita A., Yamamoto S., *ET AL.*: 'Molybdenum substitutional doping and its effects on phase transition properties in single crystalline vanadium dioxide thin film', *Appl. Phys.*, 2013, **86**, p. 5311
[47] Jin P., Tanemura S.: 'V1-x $MoxO_2$ thermochromic films deposited by reactive magnetron sputtering', *Thin Solid Films*, 1996, **281**, p. 239
[48] Jian J., Chen A., Zhang W., *ET AL.*: 'Sharp semiconductor-to-metal transition of VO_2 thin films on glass substrates', *Appl. Phys.*, 2013, **114**, p. 244301

doi: 10.1049/mnl.2019.0186